Copper(II) Azide Complexes of Aliphatic and Aromatic Amine Based Tridentate Ligands: Novel Structure, Spectroscopy, and Magnetic Properties

P. Manikandan, R. Muthukumaran, K. R. Justin Thomas, B. Varghese, G. V. R. Chandramouli, and P. T. Manoharan*

Department of Chemistry and Regional Sophisticated Instrumentation Centre, Indian Institute of Technology Madras, Chennai-600 036, India

Received August 11, 2000

Copper(II) azide complexes of three tridentate ligands namely 2,6-(3,5-dimethylpyrazol-1-ylmethyl)pyridine (L), 2,6-(pyrazol-1-ylmethyl)pyridine (L′), and dipropylenetriamine (dpt) yield three kinds of complexes with different azide-binding modes. The ligand L forms two end-on-end (μ-1,3) diazido-bridged binuclear complexes, $[CuL(\mu\text{-}N_3)]_2(ClO_4)_2$ (**1**) and $[CuL(\mu\text{-}N_3)(ClO_4)]_2{\cdot}2CH_3CN$ (**2**), and L′ forms a perchlorato-bridged quasi-one-dimensional chain complex, $[CuL'(N_3)(ClO_4)]_n$ (**3**) with monodentate azide coordination. The ligation of dipropylenetriamine (dpt) gives a end-on (μ-1,1) diazido-bridged binuclear copper complex $[Cu(dpt)(\mu\text{-}N_3)]_2(ClO_4)_2$ (**4**). The crystal and molecular structures of these complexes have been solved. Variable-temperature EPR results of **1** and **2** are identical and indicate the presence of both ferromagnetic and antiferromagnetic interactions within the dimer, the former dominating at low temperatures and the latter at high temperatures. The unusual temperature-dependent magnetic moment and EPR spectra of this dimer reveal the presence of temperature-dependent population of two triplet states, one being caused by antiferromagnetic and the other by ferromagnetic interaction, the former transforming to the latter on cooling. While the interaction of ground spin doublets of the two metal centers gives rise to a ferromagnetic coupling of $J_g = 90.73$ cm^{-1}, the other coupling of $J_e = -185.64$ cm^{-1} is suggested to be caused by the interaction between an electron in one metal center and an electron from the azide of the other monomer by excitation of a d-electron to the empty ligand orbital. The ferromagnetic state is energetically favored by 104.39 cm^{-1}. Compound **3** exhibits axial spectra at room temperature and 77 K, and variable-temperature magnetic susceptibility data indicate that the copper centers form a weakly antiferromagnetic one-dimensional chain with $J = -0.11$ cm^{-1}. In the case of **4**, the unique presence of two nonidentical dimeric units with different bond lengths and bond angles within the unit cell as inferred by crystal structure is proved by single-crystal EPR spectroscopy.

Introduction

Studies of polynuclear transition metal complexes with interesting structural and magnetic properties have gained much interest in the recent years.[1−17] A variety of synthetic strategies have been applied to build such molecular architectures with different terminal and bridging ligands to facilitate ferro- and antiferromagnetic interactions among the metal centers.[2,5,8,9] Among the bridging ligands, pseudohalides are good choice, because of their versatile coordination behavior that generates dimeric[10,11] and multidimensional magnetic materials.[1,5,12−15]

The most fascinating aspect of the pseudohalide-bridged copper(II) polynuclear complexes is the variety in their magnetic properties.[1,5,16,18−23] As bridging ligands, depending upon the steric and electronic demand of coligands, they can change their coordination to either an end-on (μ-1,1) or an end-to-end (μ-

* To whom all correspondence should be addressed. Honorary Professor, JNCASR, Bangalore, India. E-mail: ptm@magnet.iitm.ernet.in or ptm@rsic.iitm.ernet.in. Fax: 91-044-2350509/2352545.

(1) Goher, M. A. S.; Mautner, F. A. *Transition Met. Chem*. **1999**, *24*, 454.
(2) Shen, Z.; Zuo, J. L.; Yu, Z.; Zhang, Y.; Bai, J. F.; Che, C. M.; Fun, H. K.; Vittal, J. J.; You, X. Z. *J. Chem. Soc., Dalton Trans*. **1999**, 3393.
(3) van Albada, G. A.; Smeets, W. J. J.; Spek, A. L.; Reedijk, L. *J. Coord. Chem.* **1999**, *47*, 69.
(4) Escuer, A.; Font-Bardia, M.; Penalba, E.; Solans, X.; Vicente, R. *Polyhedron* **1998**, *18*, 211.
(5) Goher, M. A. S.; Mautner, F. A. *Polyhedron* **1998**, *17*, 1561.
(6) De Munno, G.; Julve, M.; Verdaguer, M.; Bruno, G. *Inorg. Chem*. **1993**, *32*, 2215.
(7) Coronado, E.; Drillon, M.; Fuertes, A.; Beltran, D.; Mosset, A.; Galy, J. *J. Am. Chem. Soc*. **1986**, *108*, 900.
(8) Miller, J. S.; Epstein, A. J. *Angew. Chem., Int. Ed. Engl*. **1994**, *33*, 385.
(9) Entley, W. R.; Girolami, G. S. *Inorg.Chem*. **1994**, *33*, 5165.
(10) Agnus, Y.; Lewis, R.; Gisselbrecht, J. P.; Weiss, R. *J. Am. Chem. Soc*. **1984**, *106*, 93.
(11) Ribas, J.; Monfort, M.; Diaz, C.; Bastos, C.; Solans, X. *Inorg. Chem*. **1993**, *32*, 3557.
(12) Escuer, A.; Vicente, R.; Goher, M. A. S.; Mautner, F. A. *Inorg. Chem*. **1996**, *35*, 6386.
(13) Escuer, A.; Vicente, R.; Mautner, F. A.; Goher, M. A. S. *Inorg. Chem*. **1997**, *36*, 1237.
(14) Cortes, R.; Lezama, L.; Larramendi, J. S. R.; Insausti, M.; Folgado, J. V.; Madariaga, G.; Rojo, T. *J. Chem. Soc., Dalton Trans*. **1994**, 2573.
(15) Manther, F. A.; Cotres, R.; Lezama, L.; Rojo, T. *Angew. Chem., Int. Ed. Engl*. **1996**, *35*, 78.
(16) Mckee, V.; Zvagulis, M.; Dagdigian, J. V.; Patch, M. G.; Reed, C. A. *J. Am. Chem. Soc*. **1984**, *106*, 4765.
(17) Mckee, V.; Dagdigian, J. V.; Bau, R.; Reed, C. A. *J. Am. Chem. Soc*. **1981**, *103*, 7000.
(18) Kahn, O. *Molecular-Magnetism*; VCH: NewYork, 1993.
(19) Kahn, O. In *Magneto-Structural Correlations in Exchange Coupled Systems*; Willett, R. D., Gatteschi, D., Kahn, O., Eds.; D. Reidel: Dordrecht, The Netherlands, 1985.
(20) Felthouse, T. R.; Hendrickson, D. N. *Inorg. Chem*. **1978**, *17*, 444.
(21) Chaudhuri, P.; Guttman, M.; Ventur, D.; Wieghardt, K.; Nuber, B.; Weiss, J. *J. Chem. Soc., Chem. Commun*. **1985**, 1618.
(22) Kahn, O.; Sikorav, S.; Gouteron, J.; Jeannin, S.; Jeannin, Y. *Inorg. Chem*. **1983**, *22*, 2877.

10.1021/ic0009223 CCC: $20.00
Published on Web 04/07/2001

Chart 1

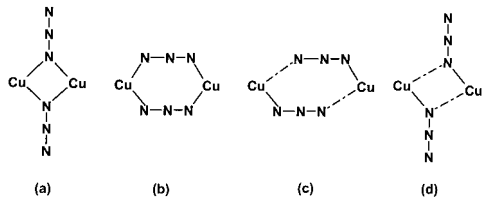

1,3) mode (Chart 1). Such azido-bridged copper(II) complexes are of great interest for biologists and bioinorganic chemists investigating the structure and role of active sites in copper proteins and for physical inorganic chemists seeking to design new magnetic materials. To understand the active sites of met-azido hemocyanins and tyrosinases many efforts have been made to synthesize azido-bridged binuclear copper complexes.[16,17] From the magnetic point of view, an unusual range of magnetic behavior can be obtained as a function of the coordination of the azide bridging group. In dibridged complexes with one or more symmetric end-on azido bridges, the interaction between the metal ions is strongly ferromagnetic,[22−24] whereas, with one or more symmetric end-to-end azido bridges, the interactions is strongly antiferromagnetic.[10,16] In complexes with asymmetric end-to-end azido bridge with short and long $Cu-N_{azide}$ bonds, the interaction is either negligible or very weakly antiferromagnetic depending on the geometry which tends to be trigonal bipyramidal or square pyramidal, respectively.[23] Complexes with asymmetric end-on azido bridge are rare, and the interaction between metal centers is weak to moderately strongly ferromagnetic.[25]

Several magneto−structural correlations have been proposed in the past few years by different groups in an attempt to get a better understanding of the influence of different parameters such as symmetry of magnetic orbitals and the nature of bridging or terminal ligands and small geometrical changes.[18,19,26,27] Among them two strategies have been proposed to achieve a ferromagnetic interaction between two metal ions belonging to the same molecular entity, namely the strict orthogonality and the accidental orthogonality of the magnetic orbitals.[19,26] These have relevance to the azido-bridged exchange coupled systems.

Electron paramagnetic resonance (EPR) spectroscopy has been shown to be very useful as a complementary method to magnetic measurements in copper(II) systems exhibiting weak magnetic interactions, since they offer more direct access to the singlet−triplet energy gap.[20,28−31] EPR spectroscopy can notably indicate large coupling through intensity variation and can also extract small coupling with the use of multifrequency experimentation.

Studies of metal complexes with tridentate ligands such as bis(pyrazolyl)pyridine-based ligands, 2,6-bis(3,5-dimethylpyrazol-1-ylmethyl)pyridine (L),[32−34] 2,6-bis(pyrazol-1-ylmethyl)-pyridine[33−35] (L′), and dipropylenetriamine (dpt),[20,36] have been of great interest for the past few years to our group for their interesting coordinating properties. In our efforts in making complexes with interesting structural and magnetic properties we report here the structure, magnetism, and detailed EPR properties of copper azide complexes with three ligands L, L′, and dpt, $[CuL(\mu\text{-}N_3)]_2(ClO_4)_2$ (**1**), $[CuL(\mu\text{-}N_3)(ClO_4)]_2\cdot 2CH_3CN$ (**2**), $[CuL'(N_3)(ClO_4)]_n$ (**3**), and $[Cu(dpt)(\mu\text{-}N_3)]_2(ClO_4)_2$ (**4**), with varying structural and magnetic properties.

Experimental Section

Materials. Commercially available reagent grade chemicals and solvents were used after appropriate purification. Dipropylenetriamine (dpt) was purchased from Fluka, 2,6-Bis(3,5-dimethylpyrazol-1-ylmethyl)pyridine (L),[32] 2,6-bis(pyrazol-1-ylmethyl)pyridine (L′),[34,35] and $CuL(ClO_4)_2\cdot H_2O$ were obtained by adopting our earlier procedure.[32,34]

Warning! Although we have experienced no difficulties with the perchlorate salts described, these compounds should be handled with appropriate precaution as perchlorate salts are known for their potential hazards.[37]

$[CuL(\mu\text{-}N_3)]_2(ClO_4)_2$ (1). To a methanolic solution (5 mL) of 59.5 mg (0.1 mmol) of $CuL(ClO_4)_2\cdot H_2O$[34] was added to 6.5 mg of NaN_3 (0.1 mmol) with constant stirring. The solution was allowed to stir for 1 h. The dark green solution formed was filtered and allowed to crystallize at room temperature to yield prismatic monoclinic crystals. The yield was 95%. Anal. Found: C, 39.92; H, 4.16; N, 22.28. Calcd for $C_{34}H_{42}Cu_2N_{16}Cl_2O_8$: C, 40.08; H, 4.23; N, 22.39.

$[CuL(\mu\text{-}N_3)(ClO_4)]_2\cdot 2CH_3CN$ (2). To a methanolic solution (5 mL) of 59.5 mg (0.1 mmol) of $CuL(ClO_4)_2\cdot H_2O$[34] was added 10 mL of aqueous solution of 6.5 mg of NaN_3 (0.1 mmol) with constant stirring. The dark green solution was allowed to stir for 1 h. The resulting precipitate was filtered out and dried. The compound was recrystallized from acetonitrile to yield prismatic crystals. Yield: 95%. Anal. Found: C, 41.92; H, 4.32; N, 22.23. Calcd for $C_{38}H_{48}Cu_2N_{18}Cl_2O_8$: C, 42.15; H, 4.47; N, 23.28.

$[CuL'(N_3)(ClO_4)]_n$ (3). An ethanolic solution (10 mL) of L' (24 mg, 0.1 mmol) was added to 37.2 mg (0.1 mmol) of $Cu(ClO_4)_2\cdot 6H_2O$ in methanol (10 mL) with constant stirring. To the resulting blue solution was added 6.5 mg (0.1 mmol) of NaN_3, and the solution was allowed to stir for 1 h. The dark green solution was filtered; slow evaporation of the solution at RT (room temperature) yielded a microcrystalline product. Yield: 95%. Anal. Found: C, 35.02; H, 2.79; N, 25.48. Calcd for $C_{13}H_{13}CuN_8ClO_4$: C, 35.14; H, 2.95; N, 25.22.

$[Cu(dpt)(\mu\text{-}N_3)]_2(ClO_4)_2$ (4). A 1.852 g amount of $Cu(ClO_4)_2\cdot 6H_2O$ (0.5 mmol) was dissolved in 20 mL of water, and 0.665 g (0.5 mmol) of dipropylenetriamine was added to it with constant stirring. The resulting limpid blue solution was added to a solution of 0.32 g (0.5 mmol) of NaN_3 dissolved in 10 mL of water. The solution was allowed to stir for 0.5 h and filtered and kept for crystallization. Dark green platelet crystals of $[Cu(dpt)(\mu\text{-}N_3)]_2(ClO_4)_2$ were obtained after 1 week which were suitable for single-crystal X-ray diffraction and EPR measurements. The yield was 95%. Anal. Found: C, 21.01; H, 5.03; N, 25.05. Calcd for $C_{12}H_{34}Cu_2N_{12}Cl_2O_8$: C, 21.43; H, 5.10; N, 24.99.

Physical Measurements. The measurements of single-crystal and polycrystalline EPR spectra were made on a Varian E-112 spectrometer using 100 kHz modulation at X-band (9.5 GHz) and Q-band (35 GHz) frequencies with DPPH a as *g*-marker. Low-temperature measurements on polycrystalline samples in X-band were carried out down to 20 K

(23) Comarmond, P.; Plumere, P.; Lehn, J. M.; Augus, Y.; Louis, R.; Weiss, R.; Kahn, O.; Morgenstern-Badarau, I. *J. Am. Chem. Soc*. **1982**, *104*, 6330.
(24) Waksman, I. B.; Boillot, M. L.; Kahn, O.; Sikorov, S. *Inorg. Chem.* **1984**, *23*, 4454.
(25) Cortes, R.; Urtiga, M. K.; Lezama, L.; Larramendi, J. S. R.; Arriortua, M. I.; Rojo, T. *J. Chem. Soc., Dalton Trans*. **1993**, 3685.
(26) Crawford, W. H.; Richardson, H. W.; Wasson, J. R.; Hodgson, D. J.; Hatfield, W. E. *Inorg. Chem*. **1976**, *15*, 2107.
(27) Livermore, J. C.; Willet, R. D.; Gaura, R. M.; Landee, C. P. *Inorg. Chem.* **1982**, *21*, 140
(28) Vicente, R.; Escuer, A.; Penalba, E.; Solans, X.; Font-Bardia, M. *J. Chem. Soc., Dalton Trans.* **1994**, 3005.
(29) Banci, L.; Bencini, A.; Gatteschi, D. *Inorg. Chem*. **1984**, *23*, 2134.
(30) Kuppusamy, P.; Manoharan, P. T. *Inorg. Chem*. **1989**, *24*, 3053.
(31) Srihari, N.; Manoharan, P. T. *J. Mol. Phys.* **1988**, *26*, 3291.
(32) Manikandan, P.; Varghese, B.; Manoharan, P. T. *J. Chem. Soc., Dalton Trans*. **1996**, 371.
(33) Manikandan, P.; Moni, M. S.; Varghese, B.; Manoharan, P. T. *J. Chem. Soc., Dalton Trans.* **1998**, 3219.
(34) Manikandan, P. Ph.D. Thesis, Indian Institute of Technology Madras, Chennai, India, 1997.
(35) Watson, A. A.; House, D. A.; Steel, P. L. *Inorg. Chim. Acta* **1987**, *130*, 167.
(36) Muthukumaran, R.; Varghese, B.; Manoharan, P. T. *First Asia-Pacific EPR/ESR Symposium*, Hong Kong, 1997; Springer-Verlag: Berlin, 1997; pp 287−294.
(37) Wolsey, W. C. *J. Chem. Educ*. **1973**, *50*, A335.

Table 1. Crystallographic Data for Compounds **1**−**4**

param	**1**	**2**	**3**	**4**
formula	$CH_{42}Cl_2Cu_2N_{16}O_8$	$C_{38}H_{48}Cl_2Cu_2N_{18}O_8$	$C_{13}H_{13}ClCuN_8O_4$	$C_{12}H_{34}Cl_2Cu_2N_{12}O_8$
fw	1000.82	1082.92	444.30	672.49
space group	$P2_1/n$	$P\bar{1}$	$P2_1/n$	$P\bar{1}$
a, Å	10.020(3)	8.393(2)	7.7155(2)	9.442(2)
b, Å	16.538(8)	12.200(4)	13.459(2)	11.472(3)
c, Å	12.758(5)	12.235(3)	16.671(3)	12.722(3)
α, deg	90.00	77.29(2)	90.00	77.14(1)
β, deg	98.68(3)	78.50(2)	100.797(10)	87.50(1)
γ, deg	90.00	79.06(2)	90	80.34(1)
V, Å^3	2089.9(14)	1183.6(6)	1700.6(4)	1324.3(5)
Z	2	1	4	2
T, K	296	296	296	296
λ, Å	0.710 73	0.710 73	0.710 73	0.710 73
ρ_{calc}, g/cm^3	1.590	1.519	1.735	1.687
μ(Mo Kα), cm^{-1}	12.16	10.81	14.82	18.68
$R(F_o)^a$	0.0602	0.0506	0.0445	0.0469
$R_w(F_o^2)^b$	0.1595	0.1449	0.1064	0.1205

[a] $R(F) = \Sigma||F_o| - |F_c||/\Sigma F_o$. [b] $R_w(F_o^2) = [\Sigma[w(|F_o|^2 - |F_c|^2)]^2/\Sigma(w|F_o|^2)^2]^{1/2}$, where $w = 1/[\sigma^2(F_o^2) + (0.066P)^2 + 2.6P]$ and $P = (\max(F_o^2, 0) + 2F_c^2)/3$.

using a closed cycle cryostat, model 22C cryodyne refrigeration systems which consists of a model 22 cold head from RMC Cryosystems and a model TG-120P temperature controller from Lake Shore Cryotronics. Calibration of temperature has been made by using a gold (0.07% Fe)−copper thermocouple rand a multimeter. A Varian variable-temperature controller unit are also used for variable-temperature X- and Q-band EPR measurements down to 77 K. Elemental analyses were done using a Heraeus CHN−O rapid analyzer. Magnetic susceptibility measurement was carried out on powder sample (for compounds **3** and **4)** at an operating magnetic field of 0.1 T using MPMS Quantum Design instrument (with a SQUID detector) in the temperature range 2.0−350 K. The error in the temperature was ±0.2 K, and in the susceptibility it was within 1%. The susceptibility measurements for compound **1** were done by using a system described by Geetha and Chakravarty[38] in the temperature range 300−20 K. The magnetic susceptibility was corrected for diamagnetism using Pascal's constants and temperature-independent paramagnetism (−60 × 10^{-6} cgs units/copper atom).[39] The molar magnetic susceptibility data were fit using a nonlinear simplex fitting routine.[40,41] The function minimized was[42]

$$F = \sum_i \frac{(\chi_i^{\text{obsd}} - \chi_i^{\text{calcd}})^2}{(\chi_i^{\text{obsd}})^2} \quad (1)$$

XRD Data Collection and Structure Determination. Crystals for single-crystal X-ray diffraction study were chosen and mounted on glass fibers and transferred to an Enraf-Nonius CAD-4 diffractometer equipped with a graphite-monochromated Mo Kα X-ray source (λ = 0.710 73 Å). The unit cell parameters were determined using the method of short vectors followed by least-squares refinement of 25 well-centered reflections. Data were collected at 293 K using $\omega\angle 2\theta$ scan technique. Intensities of three standard reflections monitored every 1 h showed less than 1% variation during the data collection time. Lorentz and polarization corrections were applied, and an empirical absorption correction (DIFABS)[43] based on ψ-scans was also applied for all the three compounds. All calculations were performed on a Digital Venturies 466 personal computer for compounds **1**−**3**. For compound **4** the computations were performed using a software package "MolEN"[44] adapted on a Micro VAX3100 computer.

Table 2. Selected Bond Lengths and Angles for $[CuL(\mu\text{-}N_3)]_2(ClO_4)_2$ (**1**)

Bond Distances (Å)			
Cu−N(6)	1.965(4)	Cu−N(3)	2.027(4)
Cu−N(1)	2.074(4)	Cu−N(5)	2.015(4)
Cu−Cu	5.632(4)	N(6)−N(7)	1.181(6)
N(7)−N(8)	1.161(6)	Cu−N(8)#	2.653(6)
Bond Angles (deg)			
N(6)−Cu−N(5)	90.4(2)	N(6)−Cu−N(3)	93.5(2)
N(5)−Cu−N(3)	176.1(2)	N(6)−Cu−N(1)	171.2(2)
N(5)−Cu−N(1)	88.4(2)	N(3)−Cu−N(1)	87.7(2)
N(7)N(6)-Cu	124.8(4)	N(8)N(7)-N(6)	176.9(5)

Space groups were assigned on the basis of systematic absences and crystallographic *E*-statistics. Atomic scattering factors for neutral atoms Cu, O, N, C, and H were taken from ref 45. Anomalous dispersion was taken into account. The structure of **1**−**3** were solved by direct methods using SHELXS-86,[46] and the refinement was carried out by full-matrix least-squares methods (SHELXL-92).[47] The structure determination of **4** was carried by using Patterson and Fourier map techniques, and the refinement, by applying least-squares techniques (*F* refinement, $w = 1/\sigma^2(F) + 0.04F^2$). Atomic coordinates were refined using anisotropic thermal parameters for all non-hydrogen atoms. Hydrogen atoms are located on a difference Fourier maps.

Results and Discussion

Structural Description of Compounds 1 and 2. Compounds **1** and **2** crystallize from methanol and acetonitrile solution, respectively, as dark green prisms. The details of crystal structural determination for the compounds reported here are given in Table 1. Selected bond distances and angles for compounds **1** and **2** are given in Tables 2 and 3, respectively.

The ZORTEP[48] diagram of cationic part of **1** is given in Figure 1. There are two dimeric units, $[CuL(\mu\text{-}N_3)]_2^{2+}$, in the unit cell and are isolated by four perchlorate anions. The perchlorate ions are found to be normal though they are not coordinated to the metal ions. Within a dimeric unit, the copper(II) centers are centrosymmetrically related and are bridged by

(38) Geetha, K.; Chakravarty, A. R.*J. Chem. Soc., Dalton Trans.* **1999**, 1623.
(39) O'Conner, C. J. *Prog. Inorg. Chem.* **1982**, *29*, 203.
(40) Spendly, W.; Hext, G. R.; Himsworth, F. R. *Technometrics* **1962**, *4*, 441.
(41) Nelder, J. A.; Mead, R. *J. Comput.* **1965**, *7*, 308.
(42) Chandramouli, G. V. R.; Balagopalakrishna, C.; Rajasekharan, M. V.; Manoharan, P. T. *Comput. Chem.* **1996**, *20*, 353.
(43) Walker, N.; Stuart, D. *Acta Crystallogr.* **1996**, *A39*, 158.
(44) Fair, C. K. *MolEN*; Enraf-Nonius: Delft, The Netherlands, 1990.
(45) Cromer, D. T.; Waber, J. T. *Intemational Tables for X-ray Crystallography*; Kynoch Press: Birmingham, U.K., 1974; Vol. IV, Table 2.2B.
(46) Sheldrick, G. M. *Acta Crystallogr.* **1990**, *A46*, 467.
(47) Sheldrick, G. M. *SHELXL 93, Program for Crystal Structure Refinement*; University of Göttingen: Göttingen, Germany, 1993.
(48) Zsolnai, L.; Pritzkown, H. *ORTEP program for personal computer*; University of Heidelberg: Heidelberg, Germany, 1994.

Table 3. Selected Bond Lengths and Angles for $[CuL(\mu\text{-}N_3)]_2(ClO_4)_2\cdot 2CH_3CN$ (**2**)[a]

Bond Distances (Å)			
Cu−N(6)	1.972(3)	Cu−N(3)	2.015(3)
Cu−N(5)	2.016(3)	Cu−N(1)	2.062(3)
Cu···N(8)#1	2.627(3)	Cu···O(1)	2.941(3)
Cu···Cu#1	5.410(2)	N(6)−N(7)	1.187(4)
N(7)−N(8)	1.162(4)		
Bond Angles (deg)			
N(6)−Cu−N(3)	92.12(11)	N(3)−Cu−N(5)	174.77(10)
N(6)−Cu−N(5)	90.31(12)	N(6)−Cu−N(1)	177.50(10)
N(3)−Cu−N(1)	88.04(10)	N(5)−Cu−N(1)	89.32(11)
N(6)−Cu−N(8)#1	89.52(11)	N(3)−Cu−N(8)#1	95.69(11)
N(5)−Cu−N(8)#1	88.95(11)	N(1)−Cu−N(8)#1	92.95(10)
N(6)−Cu−O(1)	82.22(11)	N(3)−Cu−O(1)	89.32(12)
N(5)−Cu−O(1)	86.43(12)	N(1)−Cu−O(1)	95.29(11)
N(8)#1−Cu−O(1)	170.50(12)	N(7)−N(6)−Cu	121.3(2)
N(8)−N(7)−N(6)	176.7(3)	N(7)−N(8)−Cu#1	128.4(3)

[a] Symmetry transformations used to generate equivalent atoms: #1, $-x+1, -y, -z+2$.

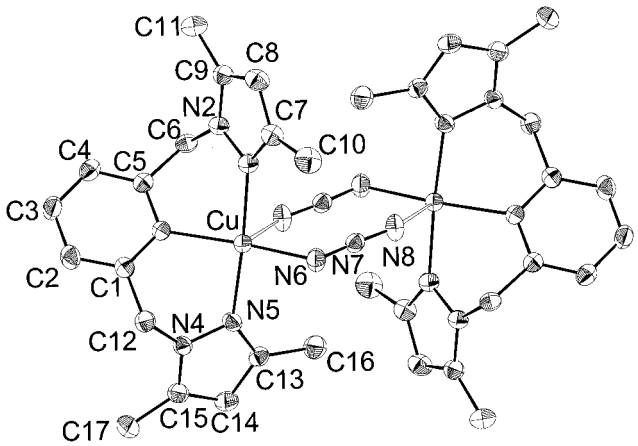

Figure 1. ZORTEP plot of the cationic part of $[CuL(\mu\text{-}N_3)]_2(ClO_4)_2$ (**1**) with atom-labeling scheme. Hydrogen atoms and perchlorate ions are not shown for clarity.

azide ions in an asymmetric end-to-end fashion. The copper(II) ion is coordinated to five nitrogens, three nitrogen atoms from the pyrazolyl and pyridine rings of L and a nitrogen atom of one of the bridging azide ($Cu-N_{azide}$= 1.965(4) Å) lying in the equatorial plane. The axial position is occupied by the second bridging azide group at a rather long distance (2.653(6) Å). The two azide ions are related by crystallographic center of inversion. The $Cu-N_{Pyrazole}$ (Cu−N(3) = 2.027(4) Å and Cu−N(5) = 2.015(4) Å) and $Cu-N_{Pyridine}$ (Cu−N(1) = 2.074 Å) distances are similar to those observed for related complexes of ligands with pyrazole and pyridine donor groups.[35] N−Cu−N bond angles vary from 88.4(2) to 176.1(2)°. The two coordinated pyrazolyl nitrogens make a biting angle of 176.1(2)° with central metal ion. Similarly, the pyridine nitrogen and azide nitrogen N(6) make an angle of 171.2(2)°. Thus the geometry around copper ion can be best described as a distorted square pyramid. The Cu···Cu distance is 5.632(2) Å. To best of our knowledge this distance is the largest reported for an azido-bridged Cu dimer thus far known except in the case of a similar compound[49] for which the reported distance was 5.774 Å though the authors were unsure of bond formation between the monomeric units. It is noteworthy that in an analogous asymmetrically bridged aliphatic triamine ligand complex $Cu_2(\mu\text{-}N_3)_2(Me_5dien)_2(BPh_4)_2$ the Cu−Cu separation is only (5.2276(7) Å).[20] The end-to-end bridging azide is quasi-linear; the N(6)−N(7)-N(8) bond angle is 176.9(5)°). The Cu−N(6)−N(7) angle is 124.8(4)°, and the

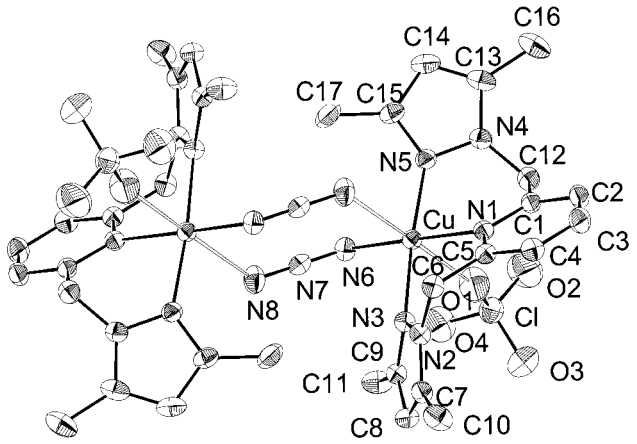

Figure 2. ZORTEP plot of $[CuL(\mu\text{-}N_3)]_2(ClO_4)_2\cdot 2CH_3CN$ (**2**) with atom-numbering scheme. Hydrogen atoms and acetonitrile molecules are not shown for clarity.

$Cu-(N_3)_2-Cu$ unit forms a chair configuration. The N−N bond lengths for the bridging azide ligand are different from one another (N(6)−N(7) = 1.181(6) Å and N(7)−N(8) = 1.161(6) Å). The pyridine and pyrazole rings can be considered as practically planar. The dihedral angle between the two pyrazoles is 72.5(2)°.

The ZORTEP[47] diagram of **2** is given in Figure 2. There is only one dimer molecule per unit cell. The structure consists of a dimeric unit $[CuL(ClO_4)]_2$ and two perchlorate anions. The dimeric unit is located about a crystallographic center of inversion. The coordination around the copper centers are very similar to that of **1** except that each copper ion has a weak coordination from one of the oxygens of the perchlorate ion at a much longer distance, 2.941(3) Å. There is an acetonitrile molecule in the asymmetric unit as a solvent of crystallization. In addition to the weak perchlorate coordination each copper has five nitrogen coordinations in similarity to **1**, three nitrogen coordination is furnished by the pyrazoles and pyridine part of the ligand Cu−N(3) = 2.015(3), Cu−N(5) = 2.016(3), and Cu−N(1) = 2.062(3) Å, and the other two are from the two azide ions. Each azide ion bridges in an end-to-end fashion. One of the azide ions is bound to copper strongly at 1.972(3) Å, while the other azide nitrogen is at a longer distance, 2.627(3) Å. The bond angle varies from 88.04(10) to 177.50(11)°. Thus, the geometry around copper can be best described as distorted octahedral when perchlorate oxygen is included. Interestingly Cu−Cu separation within the dimeric unit is only 5.410 Å, which is shorter than that of **1** by 0.222 Å. The azide nitrogens are quasi-linear (the N(6)−N(7)−N(8) bond angle is 176.7(3)°). The Cu−N(6)−N(7) angle is 121.3(2)°, and the $Cu-(\mu\text{-}N_3)_2-Cu$ unit forms a chair conformation. The difference in the two NN distances (N(6)−N(7)= 1.187(4) Å, N(7)−N(8) = 1.162(4) Å) within the azide ion is 0.025 Å. In general, the $Cu-N_{pyrazole}$ distance is shorter than the $Cu-N_{pyridine}$ length despite the fact that pyridine is more basic. This clearly indicates the rigidity of the ligand. The pyridine and pyrazole rings can be considered as practically planar. The two pyrazolyl rings have a dihedral angle of 72.6(1)°.

Structural Description of 3. Compound **3** was crystallized from acetonitrile solution as dark green prisms. The crystal and structural determination details are given in Table 1. Table 4 summarizes the significant bond distances and angles in the coordination sphere.

The structure of **3** consists of the quasi one-dimensional infinite chain system with repeating unit $[CuL'(N_3)]^+$ bridged by perchlorate anions. The ZORTEP[47] drawing with the atom-

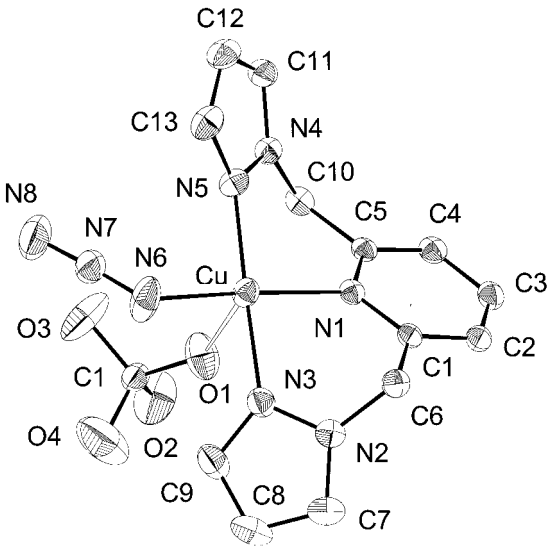

Figure 3. ZORTEP plot of monomeric view of $[CuL'(N_3)(ClO_4)]_n$ (**3**) with atom-numbering scheme. Hydrogen atoms are not shown for the sake of clarity.

Table 4. Selected Bond Distances and Angles for $[CuL'(N_3)(ClO_4)]_n$ (**3**)

Bond Distance (Å)			
Cu−N(1)	2.088(3)	Cu−N(3)	1.978(4)
Cu−N(5)	1.967(3)	Cu−N(6)	1.954(3)
Cu···Cu#1	7.7155(6)	Cu−O(1)	2.726(4)
Cu−O(2)#1	2.731(4)	N(6)−N(7)	1.171(6)
N(7)−N(8)	1.134(6)		
Bond Angle (deg)			
N(1)−Cu−N(3)	89.42(14)	N(1)−Cu−N(5)	88.97(13)
N(1)−Cu−N(6)	176.4(13)	N(3)−Cu−N(5)	178.24(14)
N(3)−Cu−N(6)	87.9(2)	N(5)−Cu−N(6)	93.7(2)
N(6)−N(7)−N(8)	177.0(6)	O(1)−Cu−N(1)	82.46(12)
O(1)−Cu−N(3)	82.1(2)	O(1)−Cu−N(5)	98.42(2)
O(1)−Cu−O(2)#1	166.49(14)	O(1)−Cu−N(6)	94.8(2)
O(2)#1−Cu−N(1)	85.00(13)	O(2)#1−Cu−N(3)	92.8(2)
O(2)#1−Cu−N(5)	86.3(2)	O(2)#1−Cu−N(6)	97.5(2)
Cu−N(6)−N(7)	126.9(4)		

labeling scheme for the repeating unit is shown in Figure 3. A view of the extended chain along is displayed in Figure 4. The chain propagates along the crystallographic *a*-axis. The copper atom is six-coordinated by the three nitrogen atoms (two pyrazolyl nitrogens and one pyridine nitrogen) of the L′ ligand, one N atom of azide ion, and two oxygens from two different perchlorates. Thus the metal ion assumes an elongated octahedron and each perchlorate ion coordinates to two metal centers. In the complex reported here the two Cu−O distances (2.726(4) and 2.731(4) Å) are indistinguishable and the bond may be considered as "semicoordinated" as Hathaway and his group proposed.[50] The O1−Cu−O2# bond angle is 166.49 (14)°. The pyridine and pyrazole rings can be considered as practically planar. The pyridine ring makes dihedral angles 53.1(1) and 56.2(2)° with the two pyrazole rings N(4)N(5)C(13)C(14)C(15) and N(2)N(3)C(7)C(8)C(9), respectively. The two pyrazole rings are inclined to each other at a dihedral angle of 65.3(2)°. All these dihedral angles and the $Cu-N_{pyrazole}$, $Cu-N_{azide}$, and $Cu-O_{perchlorate}$ bond lengths are smaller than those found in copper(II) azide complexes of methylated ligand, L (**1** and **2**). Strains due to these short dihedral angles and short Cu−N and Cu−O distances could have perhaps avoided the formation of dimers and hence the preference for a quasi one-dimensional chain. The azide ion is coordinated in a terminal fashion, and the Cu−N(6)−N(7) angle is 126.9(4)°. The $Cu-N_{azide}$ (Cu−N(6)=1.954(4) Å) and $Cu-N_{pyrazole}$ (Cu−N(3) = 1.954(4) Å and Cu−N(5) = 1.967(3) Å) distances are shorter than the $Cu-N_{pyridine}$ distance (Cu−N(1) = 2.088(3) Å). If the perchlorate bridging is not considered, the geometry of copper approximates to a square planar one. The copper−copper repeating distance is 7.7155(6) Å along the chain. The N−N distances within a azide ion are not equal (N(6)−N(7) = 1.171(6) Å and N(7)−N(8) = 1.134(6) Å), and the difference between them is 0.037 Å.

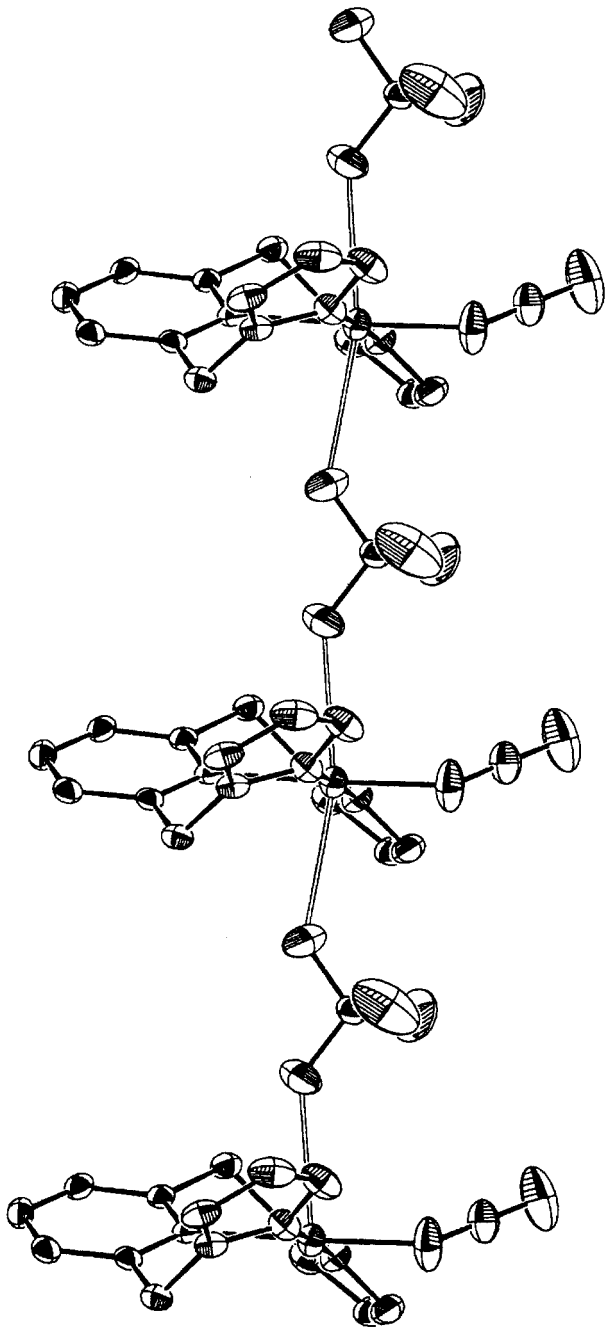

Figure 4. ZORTEP plot of $[CuL'(N_3)(ClO_4)]_n$ (**3**) along the *a*-axis. Hydrogen atoms are not shown for clarity.

Structural Description of 4. Compound **4** crystallizes from water. The unit cell contains two dimeric cations [Cu(dpt)(*μ*-

(49) Chaudhuri, P.; Oder, K.; Wieghardt, K.; Nuber, B.; Weiss, J. *Inorg. Chem.* **1986**, *25*, 2818.
(50) Hathaway, B. J. *Struct. Bonding (Berlin)* **1984**, *57*, 55.

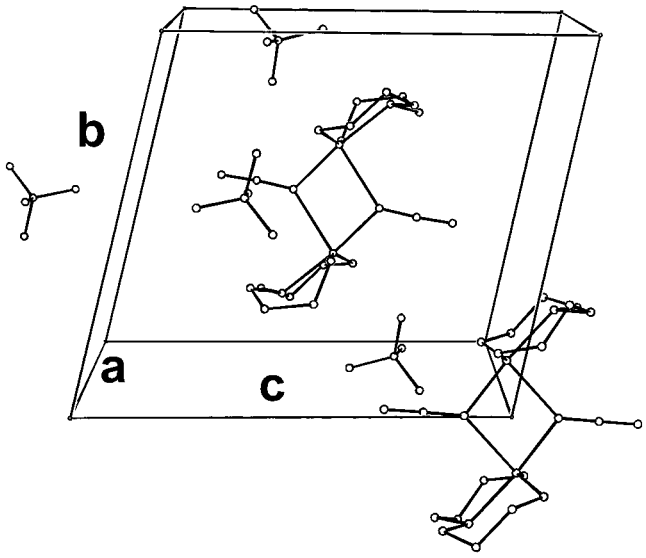

Figure 5. Packing diagram showing the non-hydrogen atoms of $[Cu(dpt)(\mu\text{-}N_3)]_2(ClO_4)_2$ (**4**).

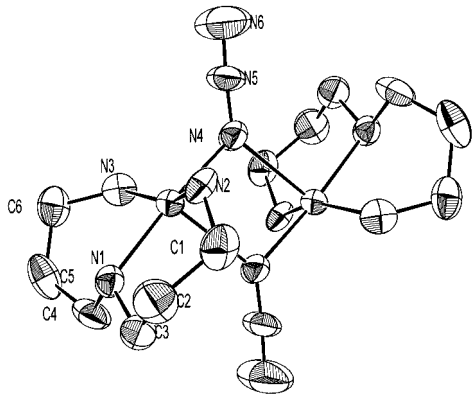

Figure 6. ORTEP diagram with 50% probability ellipsoids and atom-labeling scheme for the cation $[Cu(dpt)(\mu\text{-}N_3)]_2^{2+}$ of **4**. Hydrogen atoms have been omitted for clarity.

$N_3)]_2^{2+}$ and four noncoordinated perchlorate anions (Figure 5). The center of one dimeric cation is located about a crystallographic center of inversion. The two dimeric cations are isolated by perchlorate anion. The two cationic dimers are not identical. There are minor variations in their bond lengths and bond angles. The closest approach of two dimers seen is that of Cu(1)···Cu(2) and Cu(1)#1···Cu(2)#2 with distances 9.301(1) and 9.233(1) Å, respectively. A ZORTEP[48] view of the inner coordination about each copper(II) ion and the two bridging azide ions is shown in Figure 6. Selected bond distances and bond angles are given in Table 5. The symmetry of the coordination polyhedron of each copper(II) ion in the dimer is close to C_{4v}, which is described as a slightly distorted square-based pyramid. The elongated square-pyramidal (4 + 1) geometry of these copper(II) centers is furnished by three nitrogen atoms from the coordinated "dpt" ligand and a nitrogen atom, N(4), from one of the azide forming the basal plane, and the elongated apical position is occupied by the nitrogen from the other centrosymmetrically related azide bridge. The four coordinated nitrogen atoms in the equatorial plane are essentially coplanar. In the crystallographically independent dimers the intradimeric distances Cu(l)···Cu(1)#1 and Cu(2)···Cu(2)#2 are 3.416(1) and 3.314(1) Å, respectively.

The linear azide ions related by the molecular inversion center are bridging the two copper centers through one nitrogen atom

Table 5. Selected Bond Lengths and Angles for Compound $[Cu(dpt)(\mu\text{-}N_3)]_2(ClO_4)_2$ (**4**)[a]

Bond Distances (Å)			
Cu(1)−N(2)	2.006(4)	Cu(1)−N(4)	2.022(4)
Cu(1)−N(3)	2.024(5)	Cu(1)−N(1)	2.038(4)
Cu(1)−N(4)#1	2.398(4)	Cu(2)−N(10)	2.007(4)
Cu(2)−N(9)	2.011(5)	Cu(2)−N(7)	2.020(4)
Cu(2)−N(8)	2.042(4)	Cu(2)−N(10)#2	2.290(4)
N(4)−N(5)	1.185(6)	N(4)−Cu(1)#1	2.397(4)
N(5)−N(6)	1.135(7)	N(10)−N(11)	1.201(6)
N(10)−Cu(2)#2	2.290(4)	N(11)−N(12)	1.125(7)
Cu(1)−Cu(1)#1	3.416(1)	Cu(2)−Cu(2)#2	3.314(1)
Bond Angles (deg)			
N(2)−Cu(1)−N(4)	90.4(2)	N(2)−Cu(1)−N(3)	157.3(2)
N(4)−Cu(1)−N(3)	89.3(2)	N(2)−Cu(1)−N(1)	91.9(2)
N(4)−Cu(1)−N(1)	174.2(2)	N(3)−Cu(1)−N(1)	90.7(2)
N(2)−Cu(1)−N(4)#1	100.8(2)	N(4)−Cu(1)−N(4)#1	79.0(2)
N(3)−Cu(1)−N(4)#1	101.4(2)	N(1)−Cu(1)−N(4)#1	95.4(2)
N(10)−Cu(2)−N(9)	89.7(2)	N(10)−Cu(2)−N(7)	174.3(2)
N(9)−Cu(2)−N(7)	91.8(2)	N(10)−Cu(2)−N(8)	89.7(2)
N(9)−Cu(2)−N(8)	144.8(2)	N(7)−Cu(2)−N(8)	92.2(2)
N(10)−Cu(2)−N(10)#2	79.3(2)	N(9)−Cu(2)−N(10)#2	105.9(2)
N(7)−Cu(2)−N(10)#2	95.0(2)	N(8)−Cu(2)−N(10)#2	108.5(2)
Cu(1)−N(4)−Cu(1)#1	101.0(2)	N(6)−N(5)−N(4)	177.3(6)
Cu(2)−N(10)−Cu(2)#2	100.7(2)	N(12)−N(11)−N(10)	179.1(7)

[a] Symmetry transformations used to generate equivalent atoms: #1, $-x+1, -y+1, -z+1$; #2, $-x, -y, -z+2$.

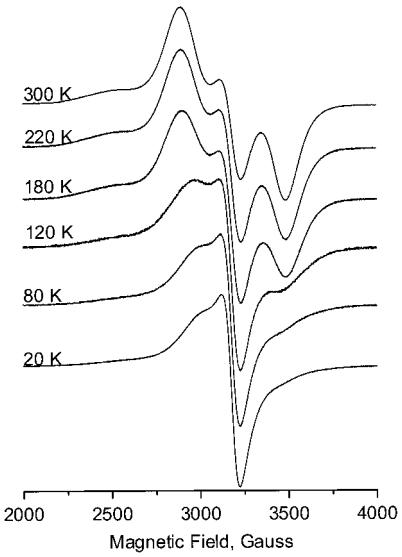

Figure 7. Representative temperature-dependent X-band EPR spectra of a polycrystalline sample of $[CuL(\mu\text{-}N_3)]_2(ClO_4)_2$ (**1**) in the region 20−300 K. The intensity scale is arbitrary.

(end-on bridging mode). Each bridging nitrogen atom simultaneously occupies an equatorial position on Cu(1) and an axial position on Cu(1)#1. The axial distance is larger (2.398(4) Å) than the corresponding equatorial one (2.022(4) Å). The angles of Cu(1)−N(4)-Cu(1)#1 and Cu(2)−N(10)-Cu(2)#2 in the bridging unit are 101.0(2) and 100.7(2)°, respectively, for each of the dimers. The perchlorate anions are, however, normal.

EPR and Magnetic Properties of 1 and 2. X- and Q-band EPR spectra have been recorded for polycrystalline samples of these azide-bridged complexes crushed from single crystals. Although there is a notable change in the crystal modifications of **1** and **2**, the EPR properties of these complexes are identical. X-band EPR spectra of monoclinic azide complex **1** and its triclinic modification **2** recorded at RT exhibit multiple signals. Though the RT spectrum, shown at the top of Figure 7, may have the look of rhombic symmetry for $S = 1/2$, it has more

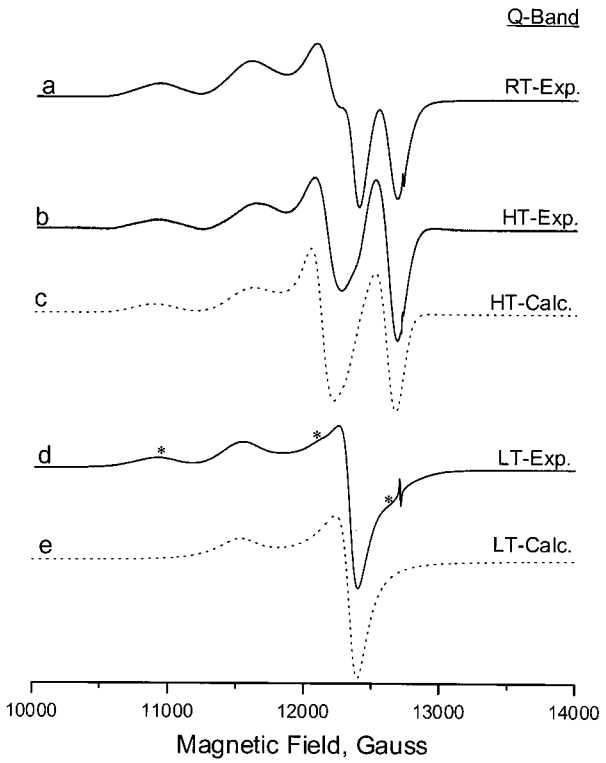

Figure 8. Q-band EPR spectra of polycrystalline sample of [CuL(μ-N_3)]$_2$(ClO_4)$_2$ (**1**): (a) at RT; (b) experimental HT component obtained by subtracting the 100 K spectrum from the RT spectrum; (c) computer simulation of (b); (d) experimental LT component (starred peaks are the remnants of HT component); (e) theoretical simulation of (d) (starred peaks are the remnant of HT components).

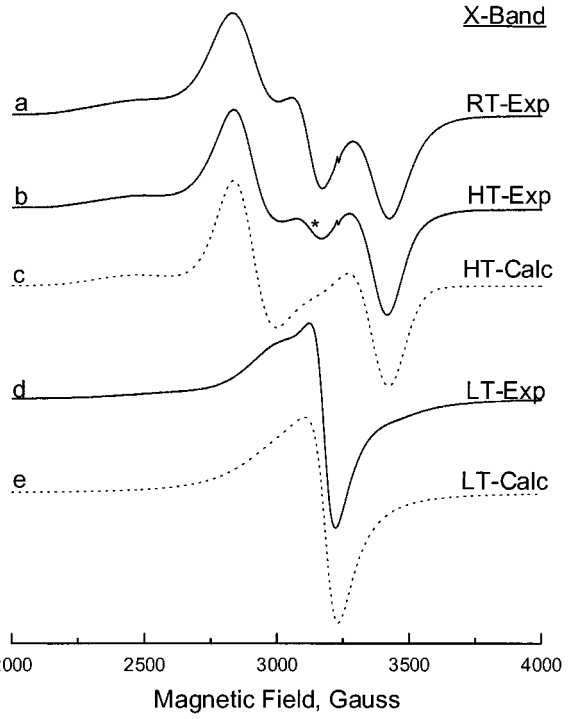

Figure 9. X-band EPR spectra of a polycrystalline sample of [CuL-(μ-N_3)]$_2$(ClO_4)$_2$ (**1**): (a) at RT; (b) experimental HT component obtained by subtracting the 80 K spectrum from RT spectrum (starred peaks are the remnants of the LT component); (c) theoretical simulation of (b); (d) experimental LT component; (e) theoretical simulation of (d).

complex character as indicated by the following: (i) The high-field line has a *g*-value much less than 2.0023. (ii) There is a half field line around 1550 G, shown in a later figure. (iii) There is an additional broad line at low field. (iv) There is a strong temperature dependence of the entire spectra. Since the spin−orbit coupling constant is negative for copper ion, one would not expect a signal of the "*g*" value less than the free electron *g*-value. Furthermore, the presence of a half field line reveals that it originates from a triplet state. Also, when this polycrystalline sample is cooled to liquid-nitrogen temperature, all other signals, except those of "*g*" values 2.0584 and 2.2070 the intensities of which increase manyfold, almost disappear.

The temperature-dependent (20−300 K) X-band EPR spectral features of **1** and **2** are shown in Figure 7 (only a few representative spectra are shown here, and the intensity is not scaled). When the sample is cooled, the intensity of one set of signals decreases gradually and almost disappears at 77 K. From 77 K and down to 20 K, there is no noticeable change in the nature of the spectrum except for a drastic increase in its intensity. Hence, two different types of signals—high-temperature (HT) lines inclusive of the one at half-field ($\Delta M_S = \pm 2$ line), almost disappearing around 77 K, and low-temperature (LT) signals, sustaining in the entire temperature region from RT to 20 K—are present. The possibility for the presence of monomeric impurity is rejected since all X- and Q-band measurements were done with the use of crushed samples of repeatedly recrystallized single crystals with highly reproducible spectral behavior. Since the interdimer separation is more than 10.5 Å, these interactions should have come only from within the dimeric unit. Also, the possibility of a breakdown of the crystal structurally observed dimers into monomers on heating or cooling is ruled out by the totally reversible temperature-dependent EPR spectral behavior in the temperature region of 20−473 K, demonstrating the integrity of the dimer in the lattice.

The room-temperature Q-band polycrystalline EPR spectrum is more resolved (Figure 8a). On cooling of the sample to 100 K (lowest achievable temperature for Q-band in our laboratory), the pattern of intensity change follows a similar trend as at X-band; i.e. the intensities of signals of "*g*" values of 2.2070 and 2.0584 (the LT signals) keep increasing and all other signals gradually reduce in intensity and more or less disappear at lower temperature (∼100 K) as represented in Figure 8d. As it is clearly seen in X-band variable-temperature EPR, the LT component is predominantly present at 77 K and signals due to both are present at RT. The low-temperature (LT) component of the X-band spectrum (as measured at 20 K) has been subtracted from the RT spectrum (Figure 9a), and the resultant component (HT) is shown in Figure 9b. Similarly, the high-temperature and low-temperature (∼100 K) components have also been separated in Q-band spectra (Figure 8b,d). High-temperature components of both X- and Q-band spectra have been successfully simulated theoretically (Figures 9c and 8c).[51] The HT model assumes axial anisotropy with zero-field splitting with the parameters $g_\perp = 2.0565$, $g_\parallel = 2.2635$, and $r = 3.96$ Å ($D^{dip} = 0.0357$ cm^{-1}),[52] where "*r*" is the distance between interacting electron centers (it should be noted here that the Cu−Cu distance is 5.632(2) Å according to the crystal structure!) (vide infra). The LT components of both X- and Q-band spectra have also been simulated theoretically with an assumption of negligible zero-field splitting and $g_\parallel = 2.2070$ and $g_\perp = 2.0584$ as seen in Figures 9e and 8e. The presence of starred peaks in Figure 8d is the remnant of the HT component since the lowest temperature Q-band measurements were done only at 100 K. It

(51) Smith, T. D.; Pilbrow, J. R. *Coord. Chem. Rev.* **1974**, *13*, 173.
(52) Sreehari, N.; Manoharan, P. T. *Mol. Phys.* **1988**, *63*, 1077.

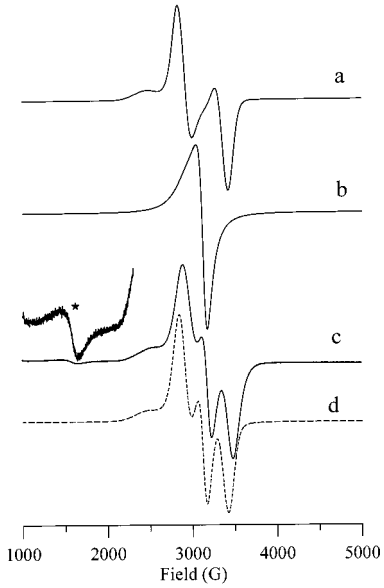

Figure 10. (a) Theoretically simulated X-band polycrystalline EPR spectrum of the HT triplet using $g_{\|} = 2.2635$, $g_{\perp} = 2.0565$, and $r = 3.96$ Å ($D^{dip} = 0.0357$ cm^{-1}) without showing the $\Delta M_s = \pm 2$ transitions. (b) Theoretically simulated X-band polycrystalline EPR spectrum of the LT triplet using $g_{\|} = 2.207$ and $g_{\perp} = 2.058$. (c) Experimental X-band EPR spectrum of polycrystalline compound **1** at RT inclusive of half-field line (asterisk). (d) Sum of 41.6% LT and 58.4% HT component to simulate (c).

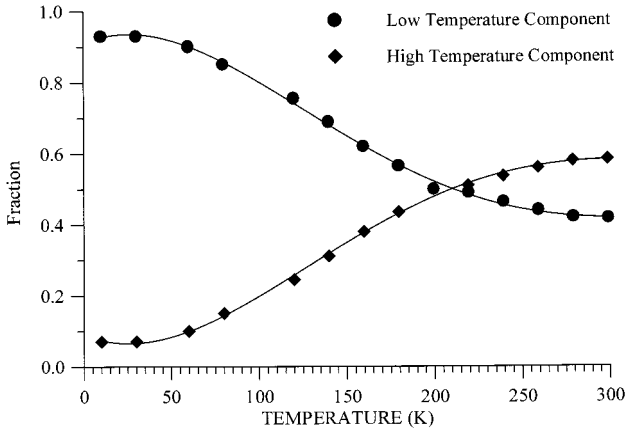

Figure 11. Fractional variation of the HT and LT triplet components as detected by EPR in **1** and **2** as a function of temperature.

may be seen that the X-band EPR spectrum at 77 K reveals the disappearance of most parts of the HT component. It is worth mentioning at this point that the similarity between the subtracted HT and LT components in Figure 8b,d and their respective simulations in Figure 8c,d testifies to the correctness of the fit and hence the parameters.

Despite our almost successful identification of the HT and LT components, a closer look reveals that both components are present at all temperatures down to 20 K. Hence, we calculated the compositions of HT and LT components in the temperature region 20−300 K by addition of the components as shown in Figure 10 in which Figure 10a,b shows the computed HT and LT components, respectively, Figure 10c the actual experimental X-band 300 K spectrum along with the half-field line, and Figure 10d the added spectrum with 58.4% HT and 41.6% LT parts. Such fractional variation of both the components as a function of temperature (20−300 K) is shown in Figure 11.

Hence these excellent fits of the experimental X- and Q-band spectra with the same parameters are clear proof of the correctness of the interpretation as well as of the fit parameters. The EPR data thus reveal the following: (i) Two different triplet states exist. (ii) The intensities of both are highly temperature dependent. (iii) As we change the temperature, one component appears to transform into the other, though one has a large zero-field splitting (ZFS) and that of the other almost negligible. However, that the LT component is also a triplet is revealed by a small splitting of $g_{\|}$ line in single crystals indicating that ZFS in the LT component is just 1/10 of that in HT component. Furthermore, the triplets in these can be generated only by a coupling of the Cu^{2+} centers within the dimer. It is obvious from the temperature-dependent intensity data that HT triplet is created as a result of antiferromagnetic interaction while LT triplet is created by ferromagnetic interaction. A rough estimate of $2J$ values for both can be obtained from their individual EPR intensity data, shown in Figure 11. We represent these interactions as J_e and J_g (respectively for HT and LT coupling), which were estimated as ∼−190 and ∼60 cm^{-1}.

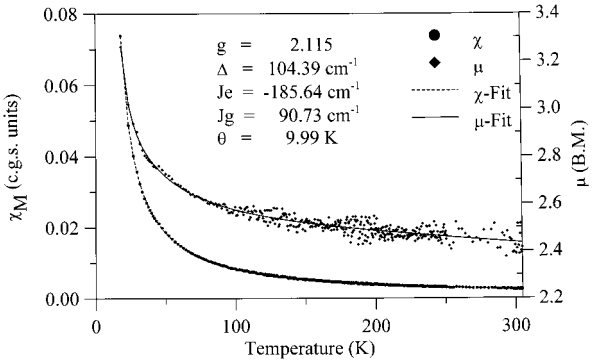

Figure 12. Experimental and theoretical molar susceptibility and magnetic moment per dimer (●/◆, experimental; —, theoretical) of $[CuL(\mu\text{-}N_3)]_2(ClO_4)_2$ (**1**). The fit was obtained using eq 2.

The correctness of the suggested electron interaction in this dimer in the manner explained above does get its added proof by the fit of the magnetic susceptibility data which are otherwise difficult to fit by any other simple dimer models, given the nature of isolated dimers revealed by crystal structure. The magnetic susceptibility measurement has been done down to 30 K. The molar susceptibility and magnetic moment per dimer are plotted against temperature (Figure 12). At room temperature the magnetic moment is 2.43 μ_B for the copper dimer, a value lower than the spin-only value, and this increases on cooling. At 30 K, the observed magnetic moment reaches 3.3 μ_B which is higher than the spin-only value of 2.73 μ_B for $S = 1$. Knowing that the total moment has contributions from two opposing interactions as evidenced by EPR, we can confidently state that this unusual magnetic behavior is the first of its kind for an azido-bridged Cu(II) dimeric complex. Magnetic susceptibility measurements have been done repeatedly to ensure reproducibility and accuracy. Since a simple dimer model could not explain this unusual behavior, we suggest the presence of a low-lying excited state with an appreciable population at RT. We propose a two-center, two-state interaction model as seen in Figure 13. Each metal center has a spin doublet ($^2\Phi_g$) as the ground state and another as the excited state ($^2\Phi_e$) (obtained by promoting one of the "d" electrons to a low-lying antibonding orbital of the azide ion). The coupling between the spin doublet ground states of the two centers will give rise to triplet−singlet states ($^3\Psi_g$ and $^1\Psi_g$) with J_g energy gap (ferromagnetic coupling) as assumed from the results of LT component of the EPR spectra. A second coupling between the spin doublet ground state ($^2\Phi_g$) of one center with the excited-state $^2\Phi_e$ of

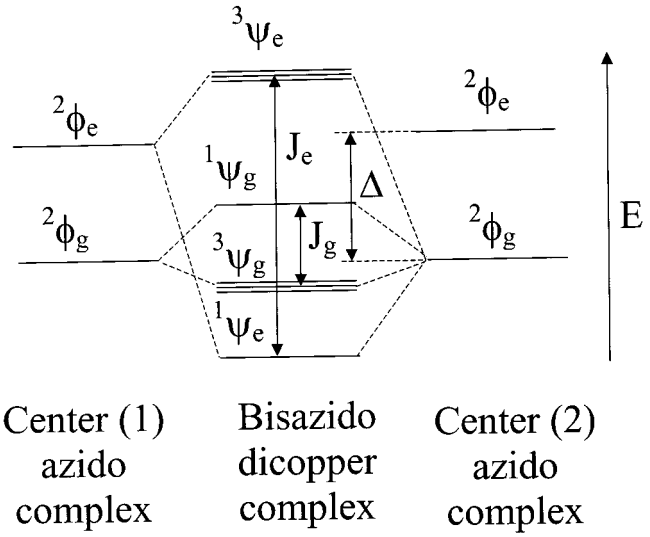

Figure 13. Proposed energy level diagram to explain the origin of exchange coupling involving the ground and excited states of two equivalent monomeric centers in $[CuL(\mu\text{-}N_3)]_2(ClO_4)_2$ (**1**).

the second center gives rise to $^1\Psi_e$ and $^3\Psi_e$ (i.e. antiferromagnetic interaction) with "J_e" energy separation. The energy derivation has been made on the basis of $H = JS_1 \cdot S_2$. The energy separation between the ground (Ψ_g) and excited (Ψ_e) states in the above model is "Δ". The susceptibility data have been fitted satisfactorily (Figure 12) with the following expression derived from the above model:

$$\chi = \frac{2Ng^2\beta^2}{k(T-\Theta)}\left[\frac{e^{-(3/4J_e-\Delta-1/4J_g)/kT} + e^{-J_e/kT}}{1 + 3e^{-(3/4J_e-\Delta-1/4J_g)/kT} + e^{-(3/4J_e-\Delta-3/4J_g)/kT} + 3e^{-J_e/kT}}\right] \quad (2)$$

The experimental susceptibility and moment data are fitted[42] with the following parameters: $g = 2.115 \pm 0.004$; $J_g = 90.73 \pm 2.36$ cm^{-1}; $J_e = -185.64 \pm 1.04$ cm^{-1}; $\Delta = 104.39 \pm 8.13$ cm^{-1}; $\Theta = 9.99 \pm 0.259$ K. The value of Θ indicates that there is an interaction between the dimers in the monoclinic lattice; the experimental evidence for this comes from the observed decrease of the EPR intensity of the LT component below 20 K, and this is attributed to a possible weak AF coupling between the dimers in the unit cell.

An attempt to include the interaction between the excited states of both centers gives poor fit of the susceptibility data, and it lacks EPR proof. Such an interaction has a lower probability. The finding of "*r*" equal to 3.6 Å (large dipolar interaction) for interelectron distance in the computer fit of HT component is approximately the distance between a copper center and the terminal nitrogen of its azide ligand (cf. the crystallographic distance between $^{\uparrow}Cu\cdots N-N-^{\downarrow}N$ is 3.846 Å). This justifies the proposal of an excited-state wave function $^2\Phi_e$ (as a result of M → L charge transfer) with an electron in the azide of L to interact with the $^2\Phi_g$ electron in the Cu^{2+} center to create the HT states. However, the LT component is due to normal interaction between the electrons from two copper centers separated by 5.6 Å and hence negligible or no dipolar interaction. Such ferromagnetic interactions have been reported and predicted in bis(azide) complexes.[53] No such earlier reports on two different triplets within the same molecule contributing to the total moment are available. However, it has been reported that the main configuration contributing to the triplet state of the end-on bis(azide) complex was found to be due to a mixing of the triplet state obtained by a single excitation to the LUMO of the N_3^- ligand.[54] Hence invoking of such an excited state in our system is not something totally new.

Another possible mechanism for this slow transformation of antiferromagnetic to ferromagnetic phase on cooling is a second-order structural phase transition which could have been caused by a conformational change from boat to chair form by the chelation rings of the tripodal ligand. This will definitely cause changes in the electronic structure of the individual copper(II) centers and in turn can alter the exchange coupling between the two centers. In this case also the same model presented in Figure 13 applies for interpreting the magnetic properties except for the following: (i) ϕ_g and ϕ_e will be termed as ϕ_1 and ϕ_2 (subscripts 1 and 2 indicating the high- and low-temperature structural phases), and hence, the interactions between the ϕ_1 centers will produce $^1\psi_1$ and $^3\psi_1$ and similarly that between the ϕ_2 centers will yield $^1\psi_2$ and $^3\psi_2$. (ii) J_e and J_g will be replaced by J_1 and J_2, and Δ will remain the same but it becomes the energy required to change phase 2 to phase 1. It must be said that this does not in anyway change expression (2) and hence the susceptibility. Though such ligand dynamics have been monitored by the NMR of copper(I) complexes[32,33] of this same ligand, we do not have any structural proof in the solid state and hence we propose the earlier mechanism as more plausible. It is worth mentioning at this point that this structural viewpoint is under investigation.

It is extremely gratifying to note the agreement between calculated and experimental magnetic susceptibility/moment using the model in Figure 13. Furthermore, proof from the EPR angle is very convincing. It is of interest to note that we have observed the presence of such temperature-dependent states/conformers in the Mössbauer spectroscopy of the iron complex[55] with this ligand L; our earlier report[32,33] on the presence of temperature-dependent conformations in the Cu(I) complexes of this ligand also lends further support.

Exchange coupling constants can be conveniently described as a sum of ferro- (J_F) and antiferromagnetic (J_{AF}) terms according to Kahn's model. In the case of bis(μ-1,3-azido)-copper(II) dimers, the exchange coupling is a function of several structural parameters such as dissymmetry or asymmetry of the μ-N_3 bridge, Cu−Cu distance (*r*), the nature of other ligating centers inclusive of its fluxionality, the number of such centers, and so on. To assess the magnitude and sign of exchange coupling, it must be understood that longer Cu−Cu distances reduce the overlap between the MO's bearing unpaired electron which will result in a reduction of the magnitude of J_{AF}, and hence, reduced antiferromagnetism is taken as evidence of ferromagnetic contributions. This is revealed by a comparison of dimers 1−4 in Table 6. In general, the reduced Cu−Cu distance results in a larger magnitude for antiferromagnetic *J* coupling as evidenced by the results on these dimers. However, no rigorous formulation, such as linearity of 2*J* with respect to *r*, is possible due to the presence of other factors. Similarly, a comparison of compounds 6 and 7 in this table indicates a drive toward ferromagnetism. While compound 6 looks more like a very weakly coupled ferromagnet, our dimer 7 in this table shows both characteristics (by either two state or two conformer

(53) Adamo, C.; Barone, V.; Bencini, A.; Totti, F.; Ciofini, H. *Inorg. Chem.* **1999**, *38*, 1996.

(54) von Seggern, I.; Tuczck, F.; Bensch, W. *Inorg. Chem.* **1995**, *34*, 5530.

(55) Padmakumar, K.; Manikandan, P.; Varghese, B.; Manoharan, P. T. *Inorg. Chem.*, to be submitted for publication.

Table 6. Comparison of Properties of Bis(μ-1,3-azido)copper(II) Dimers[a]

no.	dimer	r_{Cu-Cu}, Å	J, cm^{-1}	g	ref
1	$[Cu_2(Me_5dien)_2(\mu\text{-}N_3)_2]^{2+}$	5.228	−26.0	2.2	20
2	$[Cu_2(24\text{-ane-}N_2S_4)(\mu\text{-}N_3)_2(N_3)_2]$	5.145	diamagnetic	2.18	10
3	$[Cu_2(tmen)_2(N_3)_3]$	5.131	−308.6	∼2.1	24
4	$[L_2Cu_2(\mu\text{-}N_3)_2(ClO_4)_2]$	5.062	<−400	∼2.1	49
5	$[Cu_2(tmen)_2(N_3)_4]$	5.004	not coupled strongly(?)		57
6	$[LCu(N_3)_2]_2$ (L = *N*,*N*′,*N*″-trimethyl-1,4,7- triazacyclononane	5.774	dimer? $\Theta = +0.45$ K, very weak ferromagnet		49
7	present bis(μ-1,3-azido)copper(II) dimer	5.632	two states or two conformers with $J = 90.73$ and 185.64	2.115	present work

[a] Abbreviation for ligands taken from the respective references.

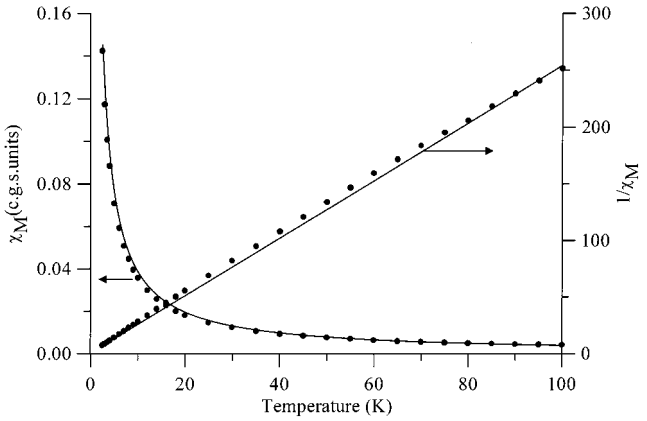

Figure 14. Experimental (···) and theoretical (—) molar susceptibility and inverse susceptibility of $[CuL'(N_3)(ClO_4)]_n$ (**3**).

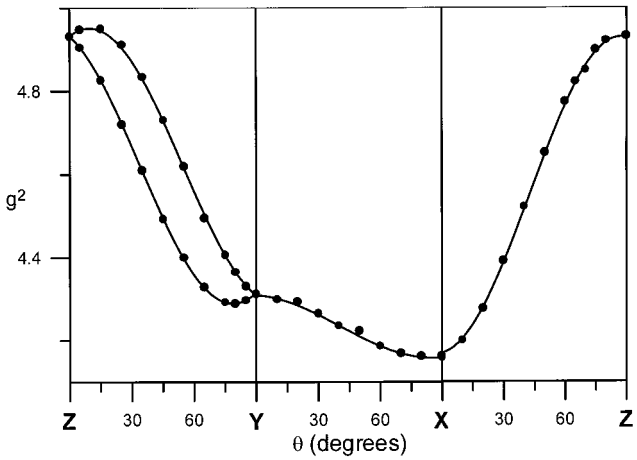

Figure 15. Plot of the angular dependence of g^2 of the single-crystal EPR spectra of $[(Cu(dpt)(\mu\text{-}N_3)]_2(ClO_4)_2$ (**4**).

model mainly due to the nature of chelation ring) but conforming to the general trend though the very large Cu−Cu distance of 5.774 Å in compound 6 weakens even the J_F contribution while this part is much stronger in compound 7 because of a shorter r_{Cu-Cu} (by 0.14 Å). The fluxionality and/or the structure of the ligand in compound 7 must have been the main driving force for the two states or two conformers with sizable contribution also coming from r_{Cu-Cu}. The general trend in structure−magnetism correlation exists but requires a careful study in future.

EPR and Magnetic Properties of 3. X-band polycrystalline EPR spectra of the compound **3** are found to be axially symmetric both at 298 and 77 K with g values $g_{\|} = 2.210$ and $g_{\perp} = 2.052$. The frozen solution EPR spectra indicate that the complex dissociates into monomeric species when dissolved in acetonitrile.

Temperature-dependent molar magnetic susceptibility and magnetic moment values of $[CuL'(N_3)(ClO_4)]_n$ are plotted and shown in Figure 14. The molar susceptibility value increases continuously when the temperature decreases to 4.2 K without any maximum. The inverse susceptibility data and the magnetic moment of 1.67−2.0 μ_B in the temperature range 2.5−100 K indicate very weak antiferromagnetic exchange interactions among the copper(II) centers along the chain which is expected for this perchlorato-bridged one-dimensional chain.

The experimental data were fit with the Bonner and Fisher numerical expression.[56] The values of the parameters g and J determined by least-squares fitting procedures are $g = 2.05$ and $J = -0.11$ cm^{-1}. The agreement factor defined by $\Sigma(\chi_{obsd} - \chi_{cald})^2/\Sigma(\chi_{obsd})^2$ equal to 1.4×10^{-5} is an indication of an excellent fit.[42] Though we have measured the susceptibility for the region 2−300 K, the fitting shown in Figure 14 is restricted to 2−100 K. Introducing interchain exchange gives a poor fit. This suggests that this perchlorate-bridged azide compound acts as a one-dimensional weak antiferromagnetic chain with almost zero interchain exchange interaction. It is necessary to point out that a fit assuming it to be a simple paramagnet turned out to be poor.

EPR Spectroscopy of 4. The X- and Q-band polycrystalline EPR spectra of the magnetically concentrated sample were recorded at RT and liquid-nitrogen temperature. There is no change in the line shape, line width, and resolution as a function of temperature. At X-band, the EPR spectra showed an axial symmetry with an asymmetry in the perpendicular region both at room temperature and at 77 K. The general features of the spectrum are similar to those for copper complexes implying a $d_{x^2-y^2}$ ground state;[57] the forbidden magnetic dipolar transitions and the singlet−triplet transitions could not be found at both temperatures. The Q-band polycrystalline spectrum at RT consists of signals with rhombic symmetry at g-values of $g_1 = 2.223$, $g_2 = 2.067$, and $g_3 = 2.037$. This pattern of g-values is suggestive of a slightly distorted square-pyramidal coordination geometry in the immediate vicinity of the copper(II) ion.

Single-crystal spectra of $[Cu(dpt)(\mu\text{-}N_3)]_2(C1O_4)_2$ were recorded both at X- and Q-band frequencies at room temperature and at 77 K. In the rotation axes frame for the single-crystal experiments on the platelike crystals of $[Cu(dpt)(\mu\text{-}N_3)]_2(C1O_4)_2$, x and y were taken parallel to [011] and [100] directions, respectively, whereas the z axis is perpendicular to both. No substantial shift in resonance field was observed upon cooling but for a small narrowing of the lines. The angular dependence of g^2 from Q-band spectral data is shown in Figure 15. A single line is observed when y and z are the rotation axes about which the crystal is rotated in the applied magnetic field, both at X-

(56) Baker, G. A., Jr.; Rushbrooke, G. S.; Gilbert,.. *Phys. Rev.* **1964**, *135*, A1272.

(57) Bkouche-Walksman, I.; Sikorav, S.; Kahn, O. *J. Cryst. Spectrosc. Res.* **1983**, *13*, 303.

Table 7. Orientation Matrices of the **g**-Tensor Principal Axis Elements with Respect to the *xyz* Frame for Compound **4**

		x	y	z
		Site 1		
g_x	2.0261	0.4371	0.8993	0.0154
g_y	2.0863	0.8995	0.4336	0.1001
g_z	2.2234	−0.0834	−0.0575	0.9949
		Site 2		
g_x	2.0225	0.4547	0.8904	0.0201
g_y	2.0891	0.8857	0.4497	0.1151
g_z	2.2246	−0.0931	−0.0701	0.9932

and Q-band frequencies. The increase in the line width, i.e., $\Delta B_{pp}{}^{Q} > \Delta B_{pp}{}^{X}$, is an indication of the presence of two different species. Increase in line width in Q-band is due to the tendencies of the two sites to have slightly differing *g*-values in these magnetic planes. In the rotation of the *yz* plane (*x*-axis rotation), two signals were observed, indicating the presence of two magnetically inequivalent sites of the copper(II) ions with the same geometry. However, in this plane, $\Delta B_{pp}{}^{Q} < \Delta B_{pp}{}^{X}$ is due to the separation of line widths and exchange interaction. Furthermore, in the $\Delta M_s = \pm 2$ region, no signal was found. The unit cell packing (Figure 5) illustrates the role of the perchlorate anions in isolating the Cu(II) dimers. As a result, the closest interdimer Cu−Cu distance (Cu(1)#1−Cu(2)#2) is 9.233 Å. This large interdimer Cu−Cu distance led to well-resolved signals of the magnetically inequivalent dimers in the magnetically concentrated lattice. No interdimer interactions could be directly detected down to 77 K. This means that interdimer magnetic exchange interactions should be minimal. This is evident if we compare the line widths of spectra obtained in the *yz* plane by X-band (35−42 G) and Q-band (22−30 G). The increased line width in X-band gives an upper estimate of interdimer exchange coupling, estimated at ∼230 MHz. This exchange must have been mediated by the perchlorate ions. Moreover, the ratio of the largest separation between the signals at Q-band (ΔB_Q) to the largest separation at X-band (ΔB_X) is equal to the ratio of the operational frequencies at Q-band to X-band, i.e.,

$$\frac{\Delta B_Q}{\Delta B_X} = \frac{290}{80} = 3.625 \quad \frac{\nu_Q}{\nu_X} \cong 3.5 \qquad (3)$$

which suggests the origin of the splitting between the signals as *g*-value anisotropy rather than zero-field splitting or any other interaction. Furthermore, the relative intensities of the two lines in the single-crystal Q-band spectra are an indication of differing singlet−triplet separations for the two sites in consonance with the crystal structural results; cf. differing interdimer Cu−Cu distances as well as other bond distances and bond angles. However, an exact estimate of the intradimer exchange coupling cannot be estimated with the existing experimental results. Detailed experiments are underway.

The analysis of the angular dependence of the g-factors using standard least-squares fit[22] leads to the tensor principal component values of $g_x = 2.026$, $g_y = 2.086$, and $g_z = 2.2234$ for site 1 and $g_x = 2.023$, $g_y = 2.089$, and $g_z = 2.2246$ for site 2. The average of these tensor component elements for the inequivalent sites ($g_x = 2.0245$, $g_y = 2.087$, and $g_z = 2.224$) are in agreement with the polycrystalline *g*-values. The orientation matrixes of the **g**-tensor with respect to the orthogonal frame *x*, *y*, *z* are presented in Table 7. The orientation of the **g**-tensor is as expected for an elongated square pyramidal copper(II) complex, with the maximum *g*-value, viz. $g_{\|} = 2.224$, observed along the axial Cu−N4#1 direction, while the other two are,

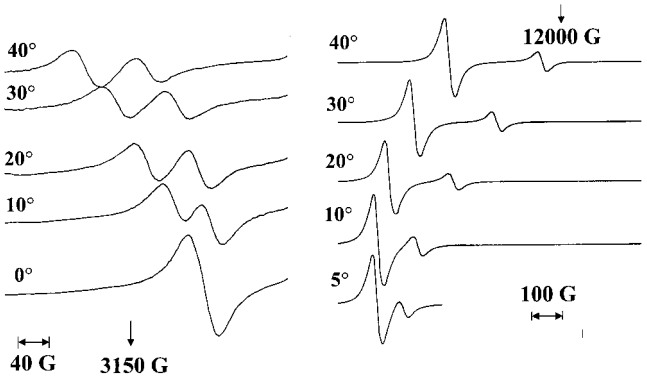

Figure 16. Single-crystal EPR spectra of $[(Cu(dpt)(\mu\text{-}N_3)]_2(ClO_4)_2$ (**4**), at the Q-band (right) and X-band (left), when the crystal was rotated about the [011] direction. 0° corresponds to the applied magnetic field parallel to the (100) axis.

Table 8. Observed Linewidth and Largest Field Separation for $[Cu(dpt)(\mu\text{-}N_3)]_2(C1O_4)_2$ (**4**) at RT

site no.	plane	X-band	Q-band
1	plane 1	single line	single line
	ΔB_{pp} (G)	60 to 80	90 to 110
2	plane 2	single line	single line
	ΔB_{pp} (G)	24 to 32	32 to 35
3	plane 3	two lines	two lines
	ΔB_{pp} (G)	35 to 42	25 to 30
	ΔB (the largest) (G)	80	290

within experimental error, along the Cu−N(1) and Cu−N(3) bond directions for site 1 and the corresponding directions for site 2 are along the Cu−N(11), Cu−N(7), and Cu−N(9) bonds, respectively.

The EPR data also give valuable information concerning magnetic exchange pathways. The narrow line width (Table 8) with a ΔB_{pp} not exceeding 80−82 G at room temperature and the Lorentzian line shape observed in all magnetic planes indicate that an exchange-narrowing regime is operative. The exchange interaction is strong enough to produce a complete merging of the hyperfine splitting lines as is evident from the Lorentzian line shape, but it does not average the signals from the two magnetically inequivalent sites. Assuming that the parallel hyperfine splitting is at least 120×10^{-4} cm^{-1}, the exchange coupling between magnetically equivalent sites *(intradimer* coupling) must be at least 45×10^{-4} cm^{-1} to completely average out. The results clearly suggest that the exchange interaction between magnetically equivalent sites (intradimer coupling) are much more efficient than that between inequivalent ones (interdimer coupling). The interaction between inequivalent sites *(interdimer* coupling) is minimal but not zero. The intensities of the two signals at Q-band were unequal, with one being broad and low in intensity, while the other one is relatively sharper and larger in amplitude (Figure 16). The observation of unequal line widths from the magnetically inequivalent dimers is indicative of difference in the strength of exchange coupling in these two dimers which are part of the same unit cell. The presence of such inequivalent molecular moieties has been a subject of recent EPR investigation.[58]

Magnetic Susceptibility of 4. The thermal evolution of the reciprocal susceptibility and $\chi_m T$ of $[Cu(dpt)(\mu\text{-}N_3)]_2(C1O_4)_2$ in the range 2−260 K are shown in Figure 17. Magnetic measurements were made out of polycrystalline samples obtained by crushing large single crystals. The temperature-dependent data

(58) Wijnands, P. E. M.; Wood, J. S.; Reedijk, J.; Maaskant, W. J. A. *Inorg. Chem.* **1996**, *35*, 5, 1214.

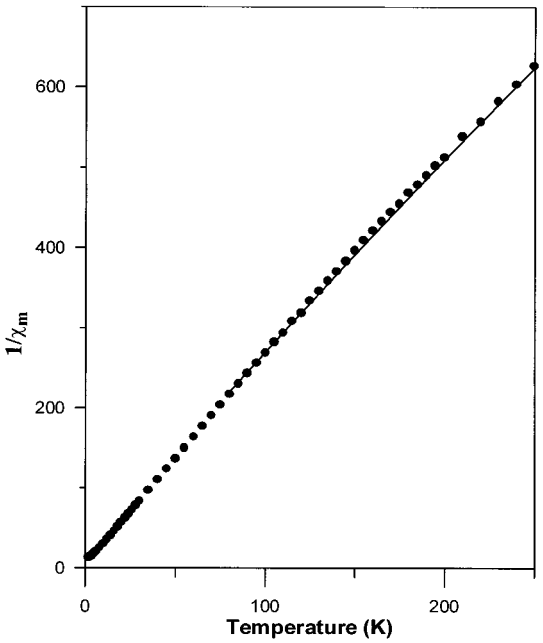

Figure 17. Plot of inverse magnetic susceptibility versus temperature for $[(Cu(dpt)(\mu\text{-}N_3)]_2\ (ClO_4)_2$ (**4**). The solid line was generated from the best-fit magnetic parameters as described in the text.

($T > 70$ K) were fitted to a Curie−Weiss law, the Weiss temperature being $\Theta = -4.23$ K with the Curie constant 0.759 cm^3 K mol^{-1} ($g = 2.012$). This variation may be indicative of weak antiferromagnetic interaction. Moreover, the absolute value of exchange coupling constant, $|J|$, is less than 1 cm^{-1} in agreement with EPR results. The weakness of the magnetic coupling (intradimer coupling) is such that J is too small in magnitude to be measured by the magnetic susceptibility technique. This is in accordance with the previous results.[26] The magnetic exchange coupling constant, J, can be expressed as a sum of both ferromagnetic (J_F) and antiferromagnetic (J_{AF}) contributions,

$$J = J_F + J_{AF}. \tag{4}$$

While the ferromagnetic contribution is usually small, the magnitude of the antiferromagnetic part is proportional to the overlap integral, S, between magnetic orbitals, $J_{AF} \propto S$. Therefore, the resulting sign of the magnetic interactions will depend to a greater extent on the amplitude of that overlap. Magnetic coupling between copper(II) ions in dimers with this type of structure appears to be weak, and it can be considered that it is not apparent in the molar magnetic susceptibility curve. This is not surprising, taking into account that in $[Cu(dpt)(\mu\text{-}N_3)]_2(C1O_4)_2$ the exchange pathway lies on a normal to the magnetic orbital. From the crystal structure it can be seen that the exchange interactions between the copper(II) pairs are propagated through the asymmetrically bridged end-on azide ions. The geometry of the dimeric cation $[Cu(dpt)(\mu\text{-}N_3)]_2^{2+}$ is unfavorable to transmit the exchange interaction effectively. In a copper(II) environment that is an ideal square pyramid the exchange coupling constant would be zero due to the fact that the magnetic orbitals are essentially localized in the equatorial planes. The distortion in the apical position permits the magnetic orbitals to acquire some type d_{z^2} admixture. The resulting weak delocalization on the apical site (*z*-direction) allows a weak interaction to occur. Thus the observed weak magnetic coupling can be explained in terms of the topology of the bridges between the copper(II) centers. For $[Cu(dpt)(\mu\text{-}N_3)]_2(C1O_4)_2$, the single-crystal EPR spectra and crystal structure were obtained at RT and the magnetic results were determined from the data in the range 2−300 K. The crystal structure reveals the asymmetric end-on azide bridging mode, while the single-crystal EPR studies confirm the presence of two magnetically nonequivalent dimers and also give valuable information concerning the possible exchange pathway. In the Q-band, two resonance lines with unequal intensities have been observed and such a phenomenon could be possible from the magnetically as well as structurally inequivalent dimers in $[Cu(dpt)(\mu\text{-}N_3)]_2(C1O_4)_2$.

Temperature-dependent magnetic susceptibility studies reveal the weak antiferromagnetic nature of the intradimer exchange coupling, while single-crystal EPR studies indicate the existence of isolated dimers with minimal interdimer magnetic exchange interactions. Though it is known that bis(azido)copper(II) dimers with end-on mode are generally ferromagnetic,[53] our result indicating this complex to be weakly antiferromagnetic is a real surprise. We, however, realize that $Cu-N_4-Cu$ and $Cu-N_{10}-Cu$ bond angles as well as the Cu−N bond lengths are substantially different for the two molecules within the unit cells. Hence, it is even possible while one unit is antiferromagnetic and the other ferromagnetic leading to the observed weak antiferromagnetism. Also, the asymmetric bridges connect an equatorial site with high spin density to an apical site which has a weak spin density. This situation is less favorable regarding the importance of spin-polarization effect and leads to the observed weak intradimer magnetic interactions.

Acknowledgment. P.M. and R.M. thank the Council of Scientific and Industrial Research (CSIR), New Delhi, India, for the research fellowships. This work was financially supported by the Department of Science and Technology, Government of India, New Delhi, by a grant (SP/S1/47/90) and by the CSIR for another grant awarded to P.T.M..

Supporting Information Available: Four X-ray crystallographic files, in CIF format, for each of the structures **1**−**4**. This material is available free of charge via the Internet at http://pubs.acs.org.

IC0009223